AIAA SciTech, 52nd AIAA Aerospace Sciences Meeting, January 2014, National Harbor, AIAA 2014–0414

Hybrid feedback design for subsonic and transonic airfoils and wings

M. Zhang[1], C. Wang[1], A. Rizzi[1], R. Nangia[2]
[1]*Royal Institute of Technology (KTH), 10044 Stockholm, Sweden*
[2]*Nangia Aero Research Associates, Bristol, UK*

A hybrid inverse/optimization method for subsonic/transonic airfoil and wing shape design is presented with application to a range of airfoil and wing cases, in preparation for the test cases defined for the Special Session of SciTech 2014. The method is hybrid in the sense that it combines the traditional inverse design technique with an optimization procedure that determines the optimum target pressure distribution. This paper emphasizes the first part, the development of SCID, the Surface Curvature Inverse Design method, the theory upon which it is based, including many of the details involved with shocks, smoothing and cross flow. The application of SCID to wing design poses many challenges, and how they are met is discussed in the context of a number of inverse design test cases for airfoils and wings. The procedure works well for airfoils, whereas twist optimization for transonic wings remains a challenge. The real benchmarks for our hybrid approach are the three Optimization Discussion Group design problems. Solutions are presented for the drag minimization of the NACA airfoil along with the wing twist optimization problem, and conclusions are drawn from the results obtained. Work has started on the drag minimization of the CRM wing in transonic flight, and final results will be presented in a future paper.

Nomenclature

α	Angle of attack
ΔC_p	C_p^*(target surface)-C_p(actual surface)
λ	Wing aspect ratio
ρ	Air density
c	Surface curvature
C_D	Drag coefficient
C_L	Lift coefficient
C_M	Moment coefficient
C_p	Pressure coefficient
M	Mach number

I. Introduction

A. Aerodynamic design approaches

Aircraft design activities are concerned with the determination of designs that meet a priori specified performance features of the vehicle. The specified design objectives are traditionally met through an iterative process of analyses, evaluations and modifications of the design. In this sequential trial-and-error procedure,

the designer must rely on experience, intuition and ingenuity for every re-design, and this makes aircraft design an exciting creative discipline. In practice, however, designers are often forced to depend on tried concepts to cut a path through an incomprehensible number of feasible designs, historically characterizing the process as a slow gradual improvement of existing types of concepts.

The revolution in computing speed and memory capacity of digital computers together with persistent systematization of design methodology has led to tools for computational aircraft design (e.g. MDO) that aim at automation of the conventional design process through integration of numerical methods for analysis, sensitivity analysis and mathematical programming so that the best design in terms of a pre-defined criterion can be determined. Traditionally the process of selecting design variations has been carried out by trial-and-error, relying on the intuition and experience of the designer, the engineer in the loop. Increasing the level of automation by computational means has reduced, but not eliminated, the engineer-in-the-loop activities. The overall success of the design process depends heavily not only on reliability and accuracy of the computational methods but also on how well the designer has set his goals.

Computational aerodynamic design, one of the disciplinary subsets of the aircraft design process, aims directly at determining the geometrical shape of the aircraft hull that produces certain specified aerodynamic properties, with or without constraints of the geometry. Usually termed aerodynamic shape optimization (ASO), this is the subject of this paper. ASO is a very attractive technology because it replaces workable designs with optimal ones, and cuts down design times, thus enabling faster responses to the economic pressure of the marketplace.

There are two main approaches to determine the aerodynamic shape of lifting surfaces, the direct design method and the inverse design. The direct design method defines a mathematical optimization problem by an objective function such as drag, and constraints on quantities of interest, such as C_L, C_m, span loads, and root bending moment. Such an optimal design problem example to minimize the aerodynamic drag at desired design condition(s), takes the form:

$$\begin{cases} \min\limits_{\boldsymbol{a}\in\mathbb{R}^n} C_D\left(\mathbf{w},\mathbf{X}\right) \quad \text{subject to} \\ \qquad C_L\left(\mathbf{w},\mathbf{X}\right) \geq l_0\,, \\ l_1 \leq C_m\left(\mathbf{w},\mathbf{X}\right) \leq l_2\,, \\ \qquad g_j\left(\mathbf{X_\Gamma}\right) \leq 0\,, 1 \leq j \leq m\,, \\ \mathbf{R}\left(\mathbf{w}_k,\mathbf{X},M,\alpha\right) = \mathbf{0}\,, \\ \qquad \mathbf{M}\left(\mathbf{X},\mathbf{X}_\Gamma\right) = \mathbf{0}\,, \\ \qquad \mathbf{S}\left(\mathbf{X}_\Gamma,\mathbf{a}\right) = \mathbf{0}\,, \end{cases} \tag{1}$$

where $\boldsymbol{a}$ is the vector of parameters being optimized, the aerodynamic coefficients C_D, C_L and C_m denote the drag, the lift and pitching moment coefficients, l_0, l_1 and l_2 are real numbers and g_j denotes the j_{th} geometrical constraint. M and α denote the Mach number and angle of attack at desired design flight state(s). The discretized flow equations, mesh adaption equation and parametrization, respectively, are described above as systems of equations written in residual form $\mathbf{R}$, $\mathbf{M}$ and $\boldsymbol{S}$. The vector of mesh coordinates is $\boldsymbol{X}$, its restriction on the shape being deformed denoted $\mathbf{X}_\Gamma$, and the vector of all flow variables (density, velocity and pressure) at all nodes in the mesh $\boldsymbol{w}$.

Various algorithms are in use to find the optimum, ranging from gradient-based search algorithms to heuristic evolution algorithms such as Genetic Algorithms. Both of them are computationally expensive, especially when the dimension of the design space is large. Recently, adjoint methods[11,12] have been developed to speed up gradient computation for large design spaces giving significantly reduced computation cost for gradient-based searches. However, the direct mathematical optimization of the objective function is likely to converge towards some local optimum rather than the global optimum. Moreover, the CFD solver Edge[5] we use supports adjoint operator computation only for inviscid flow.

In the direct optimization the aerodynamic engineer has limited inputs. The "engineer's knobs" are to choose the constraints, i.e., l_0, l_1, l_2 and g_j. Once the optimization problem is set up, it can be solved without further reference to aerodynamics. This feature is considered as an advantage but a drawback which annihilates some of the advantage is that the search in direct optimization can be "myopic", not only in finding only a local optimum, but also in the difficulties in injecting less easily quantified know-how of the big picture in the process.

The inverse design approach, on the other hand, focuses more on *design* of the pressure distribution and

admits an "engineer in loop" to add information like experience of similar shapes to fight the "myopic" view.

The motivation for pursuing inverse design is that it is more intuitive to work with pressure distribution because engineers have significant know-how which can be embodied in the target pressures. For example, working with pressure distribution for laminar-wing design avoids the need to study boundary layer stability when the target pressures have been chosen to avoid premature separation. Aerodynamicists can choose pressures which avoid adverse properties of the pressure distributions such as

(i) leading edge pressure spikes on the upper surface which encourage leading edge flow separation;

(ii) early appearance of shock wave which increases the wave drag;

(iii) non-monotonic trailing edge pressure recovery that may promote boundary layer separation.

Aerodynamic experts of course also have qualitative information on object shape to give favorable pressure distributions. For example, a bigger leading edge radius of the airfoil flattens the suction peak in (i). A thinner airfoil generally has a delayed or weakened shock wave in transonic flow. Still, this knowledge is hard to turn into mathematical constraints in the direct optimization.

Optimization and inverse design alike need to find the numerical relationship between pressure distribution and corresponding geometry. For linear flow solvers, such as panel and vortex lattice models, the pressure distribution is immediately related to the strength of the vortex distributions Γ and the camber line slope at that point. Minimization of the induced drag becomes a quadratic minimization problem with linear constants in the Γ-variables. Inverse design is then as easy as computing the flow from the shape, as long as there *exists* a shape to produce the desired pressure. Lamar[7] and Nangia[21] show good examples of subsonic flow by classical inverse design.

For non-linear flow models the relation between local shape and local pressure is not available analytically. However, it can be computed by solving the partial differential equation adjoint to the linearized flow problem. The linearization is valid for the flow at both subsonic and transonic (locally supersonic) speed, but of course there are issues with the discontinuities at shock waves.

A method can also be based on the more approximate relationship between change in surface curvature and pressure distribution. Such a scheme was investigated by Campbell[1,2] since the eighties. A similar residual-correction approach was developed by Takanashi[3] using potential flow corrections at almost the same time. Dulikravich[8] uses a Fourier series method for the Modified Garabedian-McFadden method which is reported to speed up convergence. Recent work by Bartelheimer[10] proceeds based on Takanashi[3]'s work.

B. Hybrid approach with feedback

The paper describes a hybrid scheme which combines inverse design with optimization of the target pressure distribution based on above as shown in fig. 1. The "hybrid" means we use mathematical optimization on target pressure distributions (left) in a loop with inverse design to find the shape (right). One key point is that as the iteration proceeds, the engineer can modify the current target pressure to guide the inverse deign process.

The target pressure distribution on the wing planform is constructed by considering the span loads, isobar pattern, etc.,[3] as well as other best practice guidelines provided by experience. Keeping the engineer in the loop emphasizes wing design rather than accurate solution of a (possibly not-so-well formulated) mathematical optimization task:

Engineer in loop to minimize drag by finding the best feasible target pressure distribution, for which a feasible shape can be found by inverse design.

The flow chart of hybrid optimization is shown in fig. 2. In this work we use the CFD codes MSES[4] for airfoils and EDGE[5] for wings. In the following sections, the resulting surface curvature inverse design method called SCID is introduced. To validate the methodology, it is applied to symmetric and asymmetric airfoils and untwisted/twisted wings in subsonic and transonic inviscid flow with specified target pressure distributions. Results for test cases from the optimization workshop[15,17] are shown using hybrid/inverse design.

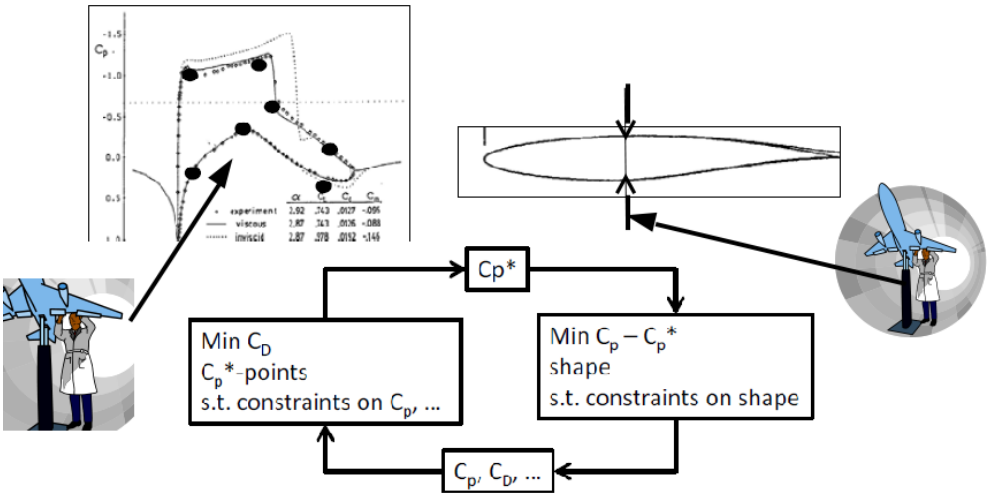

Figure 1. The feedback design loop

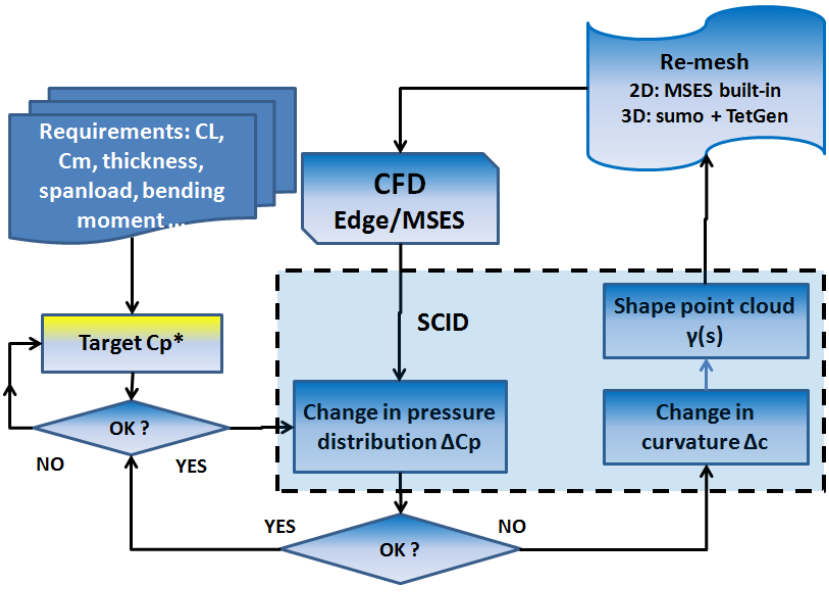

Figure 2. flow chart for wing design using SCID algorithm

II. Surface Curvature Inverse Design Method

The SCID shape design is accomplished by a variant of the CDISC procedure developed by R.Campbell.[1,2] It connects streamline curvatures on the wing surface with pressure changes to iteratively modify an initial shape. It is combined with proper under-relaxation chosen to help convergence. and a smoothing procedures used to ensure a smooth surface and curvature.

A. Theory

The relation is derived from the normal component of the momentum equation for inviscid flow along the streamline on the wing surface as long as the flow is attached. Compressibility effects of local supersonic flow have been incorporated. The momentum equation along a streamline on the wing surface is

$$UU_s\mathbf{e_s} + U^2(c_n\mathbf{e}_n + c_g\mathbf{e}_t) + \nabla p/\rho = 0 \tag{2}$$

where $\mathbf{e_s}, \mathbf{e_n}, \mathbf{e_t}$ form the Darboux frame: the unit tangent, surface normal, and $\mathbf{e_s} \times \mathbf{e_n}$ vectors, s is the *arc-length*, and c_n and c_g are the *normal* and *geodesic* curvatures of the streamline. The normal component is:

$$c_n\rho U^2 + \frac{\partial p}{\partial n} = 0$$

from which we can derive a relation between small changes in curvature and pressure coefficient,

$$\Delta c_n = \frac{c_n + 1/L}{1 - C_p} \cdot \Delta C_p$$

where L is a length-scale for the pressure gradient. A stagnation point has $C_p = 1$ so it cannot be changed by local geometry modification, but its location can move.

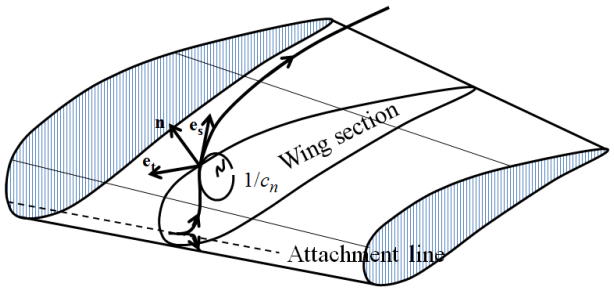

Figure 3. Wing represented in the Darboux frame

The surface analogue of the Frenet-Serret formulas for the surface coordinates $\gamma(s)$ along the streamline is

$$\gamma_{\mathbf{ss}} = c_n\mathbf{e}_n + c_g\mathbf{e}_t. \tag{3}$$

For small change on the surface, it gives

$$\Delta\gamma_{\mathbf{ss}} = \Delta c_n\mathbf{e_n} + c_n\Delta\mathbf{e_n} + \Delta c_g\mathbf{e_t} + c_g\Delta\mathbf{e_t} \tag{4}$$

where only the first term on the right hand side is kept. Note that the last two terms vanish for airfoils. The final result is the proportionality between changes in normal curvature and pressure coefficient, for unit chord-length, so curvature becomes non-dimensional,

$$\Delta c_n = F\Delta C_p \tag{5}$$

The F-coefficient was proposed by Barger and Brooks.[6] Campbell[1] suggests the c_n-dependence $F = A(1 + {c_n}^2)^B$ to produce

$$\Delta c_n = A(1 + {c_n}^2)^B\Delta C_p \tag{6}$$

where A and B are adjustable constants. A is chosen as large as possible without creating divergence in the iteration. Reported values range from 0 to 0.5. Smaller values give slow convergence, larger values may

cause divergence. The correct coefficients must be chosen as compromise between speed of convergence and robustness. An adjustment algorithm is applied to select A and B according to the status of convergence. With Δc_n from eqn. 6, the new shape $\gamma(s)$ is computed from the two-point boundary value problem.

$$\frac{d^2\Delta\gamma}{ds^2} = coeff\Delta C_p \mathbf{e_n}, \Delta\gamma(0) = \Delta\gamma(s_{max}) = 0 \tag{7}$$

The arc-length s starts from the trailing edge on the lower surface. The boundary conditions are applied to ensure a sharp and closed trailing edge. The section geometry is represented by point clouds γ_i, $i = 1, 2, ..., N$

B. Strong shock term

The convergence slows down with stronger shocks, in particular with local $M > 1.15$, so the relationship of C_p and airfoil curvature should be corrected when the flow becomes locally supersonic. Linearized theory for supersonic flow,[22] over surfaces with small angles gives

$$C_p = 2\frac{\tan\theta}{\sqrt{M_\infty^2 - 1}} \tag{8}$$

where θ is the airfoil surface angle. This can be rearranged to yield

$$\Delta C_p \mathbf{e}_n = coeff \cdot \frac{d\Delta\gamma}{ds}\mathbf{e}_n \tag{9}$$

C. Solutions

Solution of eqn.7 was done by i) geometric *exact inverse* integration and ii) second order accurate finite differences. We take airfoils for example, where the normal is the principal normal and the $\mathbf{e}_t$ terms are absent. The solution is represented by unequally spaced point clouds $\gamma(s_i), i = 1, 2, ..., N$. The arc-length-values s_i are approximated as cumulative chord-length of the polygon.

1. Geometric integration

The geometric integration method is to compute the local curvature $\frac{\partial^2\gamma}{\partial s^2}$ from the current point cloud, which is then corrected by Δc_n. The shape coordinates $\gamma(s_{i,M+1})$ for the next iteration is calculated by integration of the ΔC_p w.r.t. the arc-length s in a manner which is the *exact inverse* of the curvature-computation to avoid drift. The marching procedure needs two initial points; two linear functions of s are subsequently added to satisfy the closure constraint. The boundary conditions fix the trailing edge but the chord-length may change slightly from unit and the geometry is re-scaled as needed.

When shock waves appear, signalled by the local M exceeding a threshold (usually 1.15[1]) the relationship in eqn. 9 still holds, with the correction term for the shape surface coordinates $\gamma(s)$ related to $\frac{d\Delta C_p}{ds}$ rather than to ΔC_p. Differentiated once again w.r.t. the arc-length s, it becomes

$$k_1\frac{d\Delta C_p}{ds} = \frac{d^2\Delta\gamma}{ds^2}, \Delta\gamma(0) = \Delta\gamma(s_{max}) = 0 \tag{10}$$

This is similar to Campbell[1] CDISC procedure. However, this method has difficulties to converge towards the target pressure at transonic flow if the incidence angle is large ($> 3°$). The strong shock causes a dramatic pressure jump that, unless properly resolved, may give problems with differentiation.

2. Finite differences

The other approach is to solve the two-point boundary value problem by second order accurate finite differences.

Both subsonic and supersonic corrections are incorporated in a modification eqn. 11 of the boundary-value problem in eqn. 7

$$\beta_{ss}\frac{d^2\Delta\gamma}{ds^2} + \beta_s\frac{d\Delta\gamma}{ds} = \Delta C_p, \Delta\gamma(0) = \Delta\gamma(s_{max}) = 0 \tag{11}$$

The coefficients β_s and β_{ss} will change with geometry and local flow conditions. Campbell,[1] Dulikravich,[8] Garabedian[8] et. al. give suggestion on the choice of coefficients.

Eqn. 11, treats cases in both subsonic and transonic flow for airfoils, even with stronger shockwaves. However, the algorithm might produce self-intersecting profiles. The boundary condition only applies to constrain the trailing edge.

D. Smoothing

The numerical differencing (and subsequent summation) is sensitive to rounding errors and the computed pressure distribution is also sensitive to wiggles in the shape. Such short-wave wiggles are damped by smoothing. One version uses a least-squares approximation of the generated points by two third-order Bezier curves on both upper and lower surfaces, and another a classical global L_2-norm low-pass filter on surface coordinates. The Bezier curve shapes may not be able to represent the optimal shape exactly, but the differences are generally very small between existing airfoils and their best approximation be the Bezier curves, see e.g T.Melin.[18]

For transonic flow the pressure jump at the shock may cause the surface to bulge up in the supersonic pocket. Thus a TVD-type filter is applied to smooth the curvature.

E. Influence of cross-flow*

An attempt has been made to quantify the effect of cross-flow on the section-wise surface curvature correction process. For quadrilateral wing planform, fig. 4. The $\xi - \eta$ system represents the wing chord-wise ξ and spanwise η. Assuming an angle δ between streamlines and the chord-wise section of the wing, we obtain

$$\cos^2\delta\frac{\partial^2\Delta\gamma}{\partial\xi^2} - 2\sin\delta\cos\delta\frac{\partial^2\Delta\gamma}{\partial\xi\partial\eta} + \sin^2\delta\frac{\partial^2\Delta\gamma}{\partial\eta^2} = coeff\Delta C_p\mathbf{e_n}, \Delta\gamma(0,\eta) = \Delta\gamma(s_{max},\eta) = 0 \qquad (12)$$

This is similar to the 3D problem solved by Dulikravich[8] using a Fourier Series method. The inclusion of the spanwise derivatives addresses some of the issues discussed above. For example, the target C_p can be set up over the whole planform by interpolation from the section pressures.
However, the main point to note is that the second order spanwise derivative term is also second order small in the flow direction deviation from chordwise, but the cross-term is first order so much stronger. Earlier models such as,[8] relying on e.g. a membrane analogue, have no cross derivatives but substantial spanwise second derivatives. We conclude from this that the cross-flow effects may be limited, and that the inter-section influence of shape on pressure cannot be captured by wing surface models only.

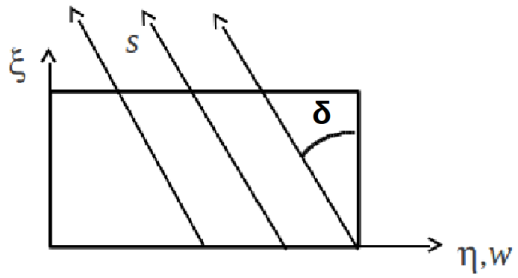

Figure 4. Wing represented in $\xi - \eta$ coordinate system

III. Challenges in wing design

The implementation of SCID for wings is more involved than just solving eqn. 7. The wing is defined from sections by lofting and NURBS surfaces, and re-meshing is needed for each design cycle. The wing tip is closed by simple G1 NURBS surface, and the trailing edge is closed. The pressure distributions from CFD solutions are extracted along the *chord-wise* sections. Wing design proceeds by matching prescribed pressure distributions at a number of span stations *as if* the flow was parallel to the section planes. The

surface curvature equations 7, 9 and/or 11 are solved for each section. Then the sections are updated, smoothed like the airfoils.

A. Challenges for SCID algorithm

There are some undetermined issues for the *chord-wise* approach that SCID algorithm is implemented:

- the cross-flow effects: if the angles between the sections and streamlines are large, the surface curvature eqn. 7, 9 and/or 11 are more inaccurate; the wing tip and leading edge are mostly influenced;
- how is the behavior at the leading edge attachment line?
- how large is the inter-section influence strength? how many sections should we use?
- stability with very small under-relaxation factor?
- the section shape update only uses section pressure data;
- how to choose/split the local α/camber change to match the C_p and C_L?

B. Challenges for engineer

The main challenge in the optimization process for the engineer is the choice of the target pressure distributions. The target C_p for the wing is chosen for each chord-wise section to ensure the wing has "straight isobars".[3] It is well known that elliptical wing loading lead to least induced drag for subsonic flow. Such constraints, as also constraints on lift and moment coefficients are easily incorporated into constraints on section-wise C_p by interpolation and integration. However, at transonic speed, the optimal loading is not known.

IV. SCID test cases

After CFD calculation of C_p for a given shape, the shape is modified by the heuristic corrector described above to approach the target pressure distribution. The corrector formula, the feed-back control for the shape, requires neither linearization of flow model nor derivatives. Hence the procedure is easily coupled to any CFD code. In this work we use the CFD codes MSES[4] for airfoils and EDGE[5] for wings. The price to pay for simplicity is the requirement for choosing the β- and A, B-coefficients, and many iterations.

In this section the design algorithm discussed above is applied to a number of test cases of airfoils and wings. The symmetric NACA0012 is selected for the all initial airfoils, and the 3D wing is rectangular without sweep. Both subsonic and transonic cases are run, proceeding from easy to hard. For the airfoils, first subsonic flow with zero-to-small angles of attack, then we proceed to transonic flow with zero-to-small angles of attack. For the wings, the easiest one is the planar wing without local twist. The most expensive case, a twisted wing with cambered airfoils in transonic flow is work in progress. Tables 1,2 give an overview of the test cases.

		TARGET			**INITIAL**		
No.	Mach	airfoil	α ($\circ$)	comments	airfoil	α ($\circ$)	comments
1	0.5	RAE100	0	-	NACA0012	0	α fixed
2	0.5	RAE2822	3	$C_L = 0.7197$	NACA0012	0	α changes
3	0.85	RAE2822	0	-	NACA0012	0	α fixed
4	0.85	RAE2822	2	$C_L = 0.7970$	NACA0012	1.5	α changes

Table 1. SCID implementations for 2D cases

		TARGET			INITIAL		
No.	Mach	airfoil	α (◦)	twist (◦)	airfoil	α (◦)	twist (◦)
1	0.5	RAE100	0	0	NACA0012	0	0
2	0.5	RAE100	0	$2 \sim 0$	NACA0012	0	$2 \sim 0$
3	0.85	RAE100	0	0	NACA0012	0	0
4	0.85	RAE2822	0	0	NACA0012	0	0
5	0.85	RAE100	0	$1 \sim -1$	NACA0012	0	$1 \sim -1$
6*	0.85	RAE2822	0	$1 \sim -1$	NACA0012	0	$1 \sim -1$

Table 2. SCID implementations for 3D cases. *Computation is ongoing with difficulties

A. SCID for airfoils

The airfoils are represented by unequally spaced point clouds in the complex plane $\gamma(s_i) = (x_i, j * y_i), i = 1, 2, ..., N$ where arclength-values s_i are approximated as cumulative chord-length of the polygon. The arc-length s starts from the trailing edge on the lower surface and ends at the trailing edge on the upper surface. The leading edge curvature is ensured to be continuous. The boundary conditions

$$\Delta\gamma(0) = \Delta\gamma(s_{max}) = 0 \tag{13}$$

ensures the airfoil a closed trailing edge. The surface curvature equation is solved with proper choice of the coefficients, which can determine the computation robustness. The new airfoil is smoothed by a low-pass filter, and this is particularly important for shocked flows.

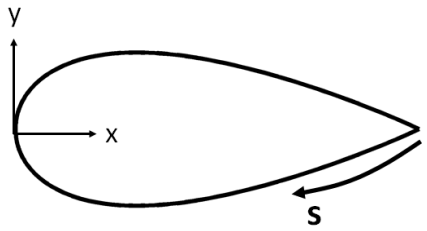

Figure 5. Airfoil streamline-following coordinate system, $\gamma(s) = (x(s), y(s))$, s is the arc-length which starts at the trailing edge on the lower surface

The following four test cases were run using MSES[4] code with the boundary layer turned-off. There are challenges involved especially for transonic flow with specified lift. Thus we proceed it from easy to hard, i.e., from subsonic to transonic, from non-lifting case to a certain lift or angle of attack. For the first three cases the angle of attack starts at zero degrees, and for the fourth case the initial angle of attack is specified as 1.5 degrees.

In the first example (fig. 6) illustrates the effect of parameter A in equation 6. The target pressure distribution is from a RAE100 airfoil at Mach 0.5 with zero angle of attack. Two design runs are made for 30 iterations, one with $A = 0.4$ and another with $A = 0.1$. The pressure distribution for the case with $A = 0.4$ matches the target quite within 0.01, with maximum deviation around the leading edge region where the pressure gradient is steep. The one with $A = 0.1$ converges more slowly especially around the leading edge with a maximum deviation (≈ 0.07). This example indicates, as expected, that a larger value of A results a more rapid convergence. Details about choice of B are found in Campbell's work.[1]

The second test case (fig. 7) is Mach 0.5 with given target lift $C_L = 0.7197$ rather than the angle of attack. MSES allows the angle of attack to change to find the given lift. The initial airfoil is NACA0012 at $\alpha = 0°$. The target pressure is from a RAE2822 airfoil at Mach 0.5 with $C_L = 0.7197$. The final design is achieved after 80 design iterations, with a stopping criterion that the maximum deviation $max|C_{p,target} - C_{p,final}| < 0.05$. Shape evolution parameters are set to $A = 0.1$ and $B = 0.4$. We can see that to match the targets, except changing in thickness, the airfoil is cambered and rotated through an angle of 2.99 degrees with a target 3

degrees. The final shape produces a $C_L = 0.725$ at the given conditions which compares well with the target one. The evolution of the airfoil surface C_p and its geometry are shown in Figure 7. We can see that the design converges quite fast from iteration 10 to iteration 50, and much more slowly from iteration 50 to the final design.

The third case (fig. 8) is to design an asymmetric airfoil in transonic flow. The target pressure is Mach 0.85 flow around a RAE2822 airfoil with zero angle of attack. The case requires 200 design cycles, with $A = 0.1$ and $B = 0.2$. The initial pressure distribution has a shock at one position for both upper and lower sides, and the modifications find the correct shock locations with reasonable computational efforts. The time for a cycle is dominated by the MSES flow solver which runs in a few seconds on a dual-core CPU.

The final test case (fig. 9) investigates the design to produce a given lift $C_L = 0.7970$ at angle of attack 2 degrees at Mach 0.85, i.e a pressure distribution from an RAE2822 airfoil for the given flow condition. The initial airfoil is NACA0012 at $\alpha = 1.5°$.

Both the initial and target airfoils have strong shocks on both upper and lower sides. The extra term $\frac{d\Delta\gamma}{ds}$ in eqn. 9 is included in the boundary value eqn. 7 for local supersonic region. The final design produces exactly the same lift $C_L = 0.7965$ as the target one. The only discrepancy from the target and the final design is that the angle of attack 2.127 degrees and 2 degrees for the target.

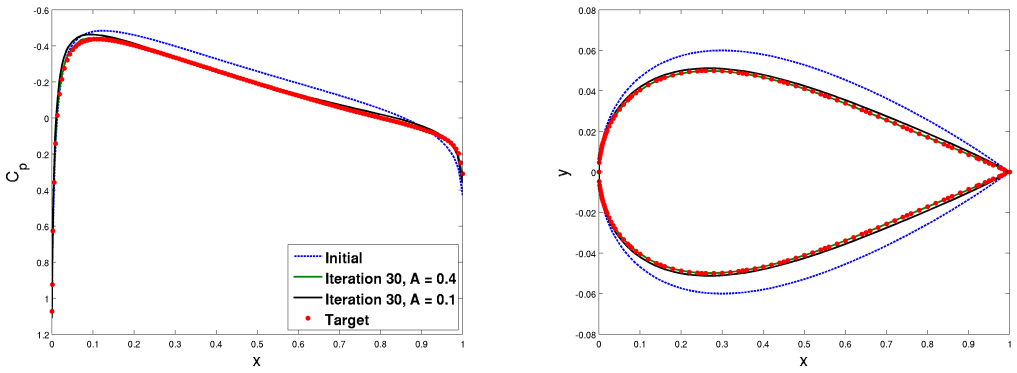

(a) Pressure distributions (b) Airfoil coordinates

Figure 6. Symmetric airfoil design case using MSES[4] at subsonic speed, M = 0.5, $\alpha = 0°$

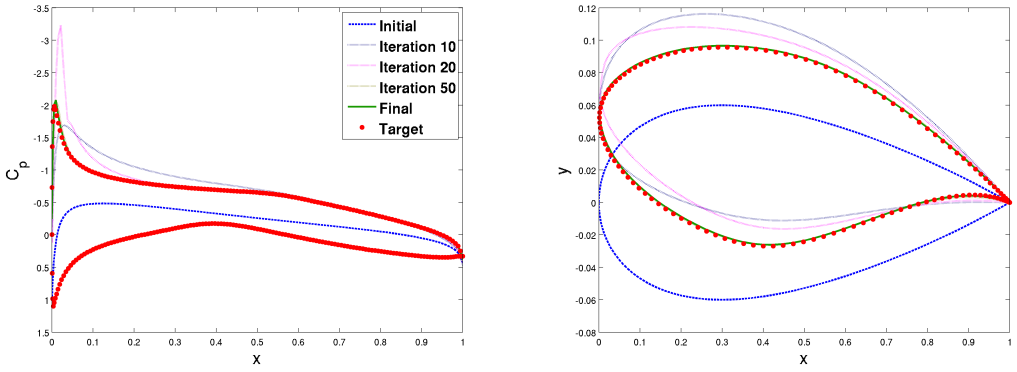

(a) Pressure distributions (b) Airfoil coordinates

Figure 7. Asymmetric airfoil design case using MSES[4] at subsonic speed, M = 0.5, $C_L = 0.7197$

B. SCID for wings

The wing surface is represented in the *sumo*[13] geometry and mesh generator by patches of Bezier surfaces built from wing sections with shapes defined by point clouds or named airfoils. *sumo* stores the cross sectional

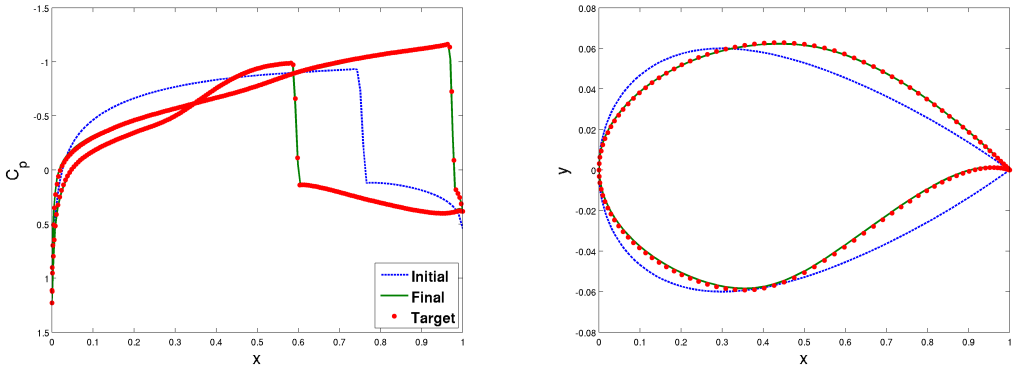

(a) Pressure distributions (b) Airfoil coordinates

Figure 8. Asymmetric airfoil design case using MSES[4] at transonic speed, M = 0.85, $\alpha = 0°$

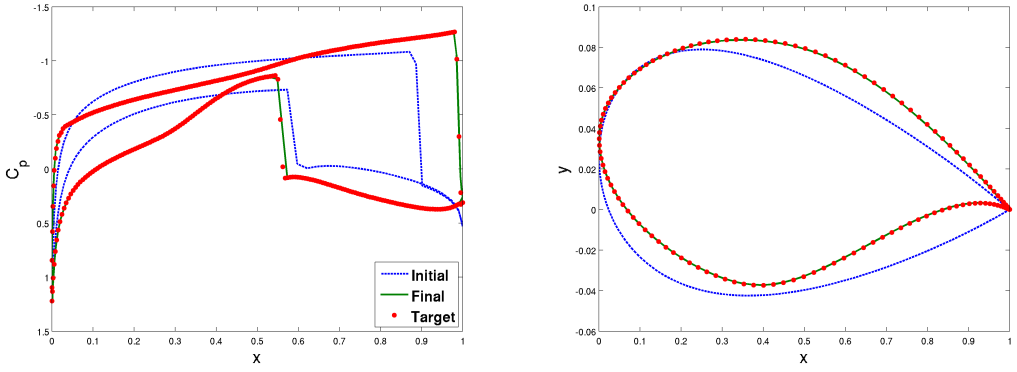

(a) Pressure distributions (b) Airfoil coordinates

Figure 9. Asymmetric airfoil design case using MSES[4] at transonic speed, M = 0.85, $C_L = 0.8$

information (point clouds) as skeletons for the components e.g., wings, fuselages, nacelles, and pylons. It allows rapid creation of aircraft geometries, automatic surface mesh generation, and automatic high-quality tetrahedral volume mesh generation by the TetGen[14] public domain software within a few minutes.

Designing 3D wings is more difficult than the two-dimensional airfoils since the streamlines does not follow the cross sections due to the cross flow. The section pressure profiles are chosen to produce desirable isobar patterns and span loading compatible with optimal drag. The shape modification includes twist and camber adjustments to impact the span loading.

There are five test cases on a straight rectangular wing with $AR = 6$. The first test case is the untwisted wing with symmetric airfoils analyzed in subsonic flow with Mach 0.5 and zero angle of attack. There are three design stations on the wing, at 0% (root),60% and 100% (tip) of the semi-span. The target wing consists airfoil sections at the design stations with RAE100 profiles. The initial wing shape has replaced the sectional profiles with NACA0012. The resulting pressure distributions and airfoil sections at design stations are shown in Figure 10, 11. The final design is obtained after 40 design cycles. The target pressure distributions at the tip section is a bit wiggled where the adverse pressure gradient starts. That is probably due to the quality of the mesh and proximity to the tip. Note that the final pressure distributions are smooth because the smoothing is applied for every cycle.

The correlation between the target pressure and the design at each station is very good, except minor discrepancies at the leading edge at the tip. The generated airfoils compare well with the target ones, except the root and tip airfoils are slightly thinner.

The second test case is also run in subsonic flow Mach 0.5 at an angle of attack zero degree with the same settings as in the first test case, but with known twist angles for each design station for both initial and target wing. The target pressure distributions are from RAE100 sections with linearly varied twist angle $2^\circ - 0^\circ$ from root to tip. The initial wing shape has the same twist angles , but the airfoils are replaced with NACA0012. Both the resulting pressure distributions and the airfoils match the target ones quite well (fig 12, 13). The local twist setting is an independent parameter other than the cross section profile shape in *sumo*.[13] In this paper all the sections are plotted as twisted.

From the third test case we start to deal with wings at transonic speed, where the "strong shock term" is involved. For the third case, the initial wing has NACA0012 airfoil, with no twist at zero angle of attack. The target pressure is obtained from an untwisted wing with RAE100 profiles at zero angle of attack at Mach 0.85, thus no lift. The shock is upstream compared to the initial one. The correct shock location is found after 50 iterations with no strong shock term incorporated. The design at 50 iteration (Iter-50) does not match the target perfectly, however it almost fits the C_p shape. Better results can be achieved by running more design cycles. .

The fourth test case is for RAE2822 airfoil at Mach 0.85, no twist and zero angle of attack. The initial wing has NACA0012 airfoils. We can see that SCID finds the correct pressure distributions at both upper and lower surfaces from root to tip after 100 design cycles. It is noticeable that in the areas of the leading edge area at the root and the tip section, which are mostly influenced by the cross-flow, SCID finds the shapes to match the target pressures nicely.

A more "realistic" twisted wing is the fifth test case. The twists are small (from 1° to -1° varied linearly) and both the initial and the target wings have the same twist angles, only wing profiles are different. We can see that the initial wing has delayed shocks. After 100 design cycles the pressure distributions match the target pressures well, although the designed sections have slightly different twist angles compared with the target ones.

C. Remarks

From the foregoing airfoil examples we see that the SCID works almost at all the conditions for both subsonic and transonic with zero-to-small angles of attack. For transonic cases when the local Mach number becomes supersonic and the strong shock term is needed to for results.

For wings, SCID works well for all subsonic conditions at subsonic, but it is much tougher when the flow becomes locally supersonic, especially hard for non-lifting airfoil with "free" twist angles as indicated of case 6 in Table 2. Each section of the wing influences each other due to the cross flow effects raised. Moreover, how to distribute the desired C_p change between the change of local angle of attack α and camber remains an unsolved problem. One possible way of solving it is to introduce spanwise terms in a wing surface curvature equation as stated in section II.E.

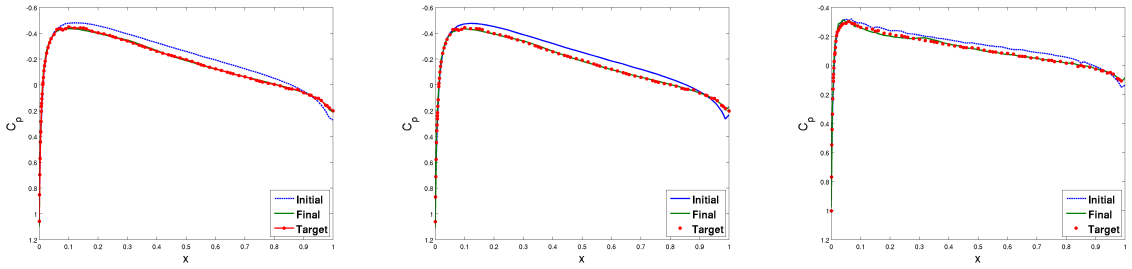

(a) Wing root (b) Wing station at 60% of the semi-span (c) Wing tip

Figure 10. Pressure distributions for rectangular wing test case, planar wing with M = 0.5, $\alpha = 0°$

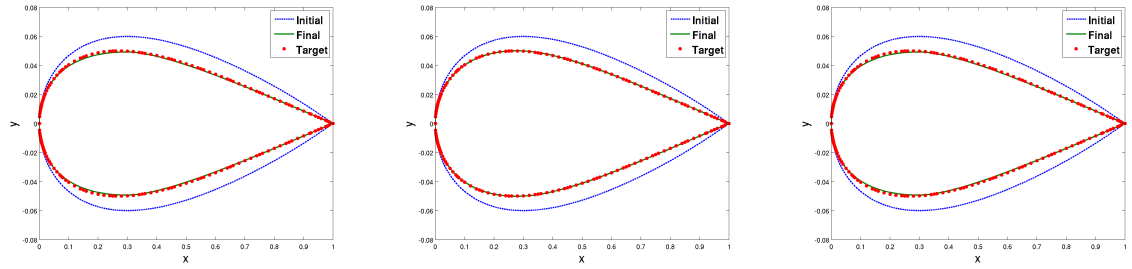

(a) Wing root (b) Wing station at 60% of the semi-span (c) Wing tip

Figure 11. Airfoil coordinates for rectangular wing test case, planar wing with M = 0.5, $\alpha = 0°$

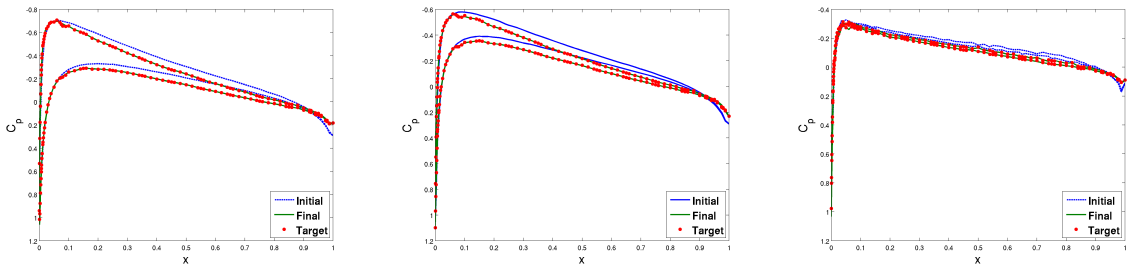

(a) Wing root (b) Wing station at 60% of the semi-span (c) Wing tip

Figure 12. Pressure distributions for rectangular wing test case at M = 0.5, wing with symmetric target wing profiles and twist angles varied linearly from 2° at the root to 0° at the tip, $\alpha = 0°$

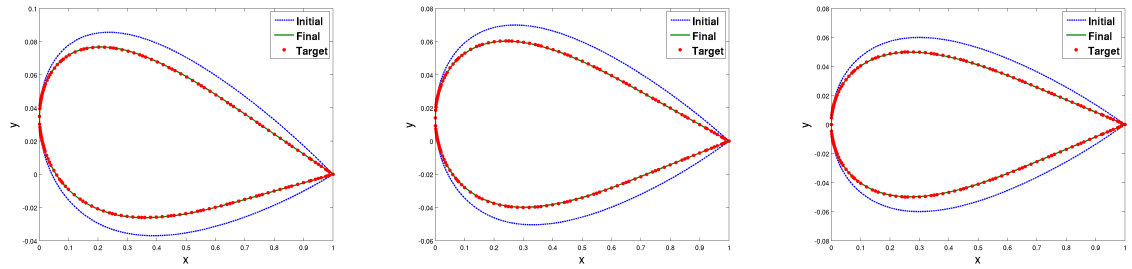

(a) Wing root (b) Wing station at 60% of the semi-span (c) Wing tip

Figure 13. Airfoil coordinates for rectangular wing test case at M = 0.5, wing with symmetric target wing profiles and twist angles varied linearly from 2° at the root to 0° at the tip, $\alpha = 0°$

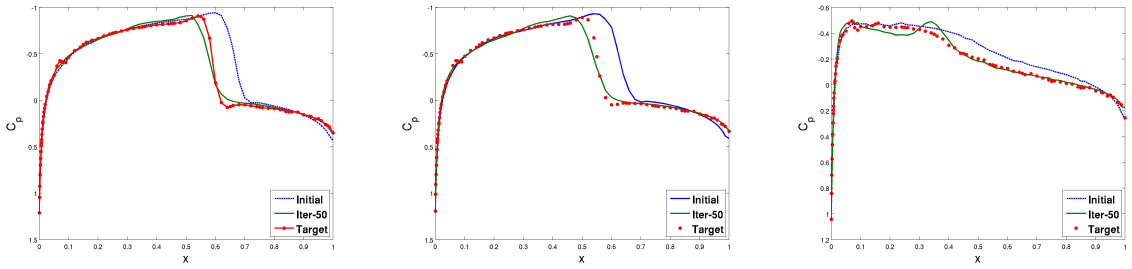

(a) Wing root (b) Wing station at 60% of the semi-span (c) Wing tip

Figure 14. Pressure distributions for rectangular wing test case at M = 0.85, planar wing with symmetric target wing profiles, at $\alpha = 0°$

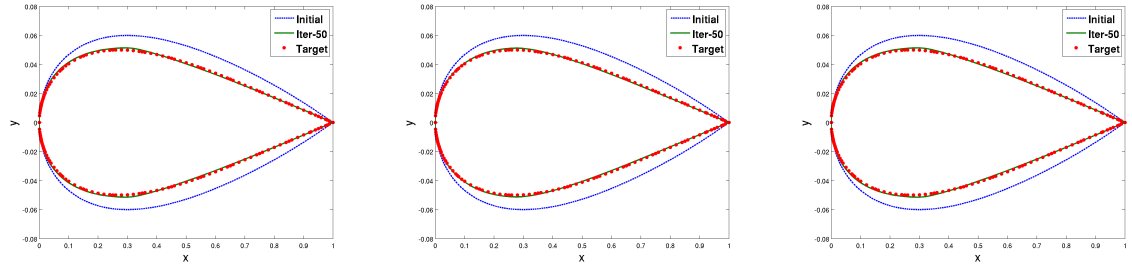

(a) Wing root (b) Wing station at 60% of the semi-span (c) Wing tip

Figure 15. Airfoil coordinates for rectangular wing test case at M = 0.85, planar wing with symmetric target wing profiles, at $\alpha = 0°$

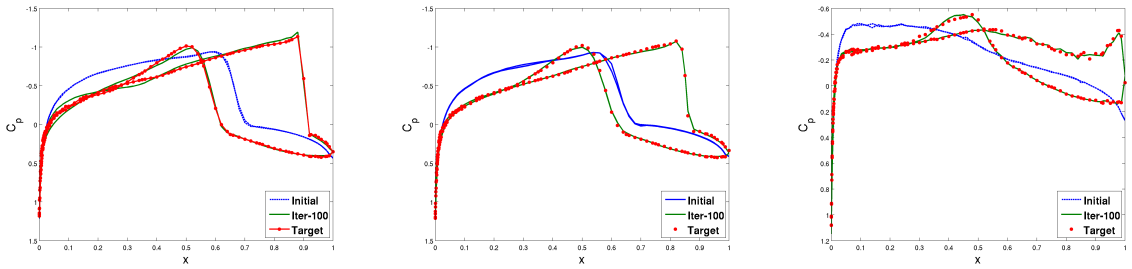

(a) Wing root (b) Wing station at 60% of the semi-span (c) Wing tip

Figure 16. Pressure distributions for rectangular wing test case at M = 0.85, untwisted wing with asymmetric target wing profiles, at $\alpha = 0^\circ$

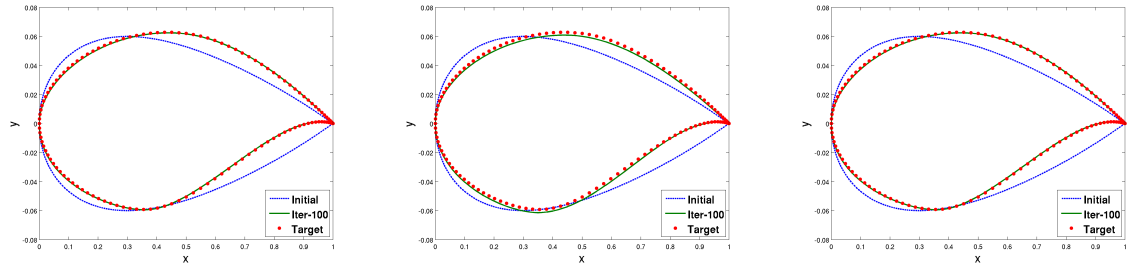

(a) Wing root (b) Wing station at 60% of the semi-span (c) Wing tip

Figure 17. Airfoil coordinates for rectangular wing test case at M = 0.85, untwisted wing with asymmetric target wing profiles, at $\alpha = 0^\circ$

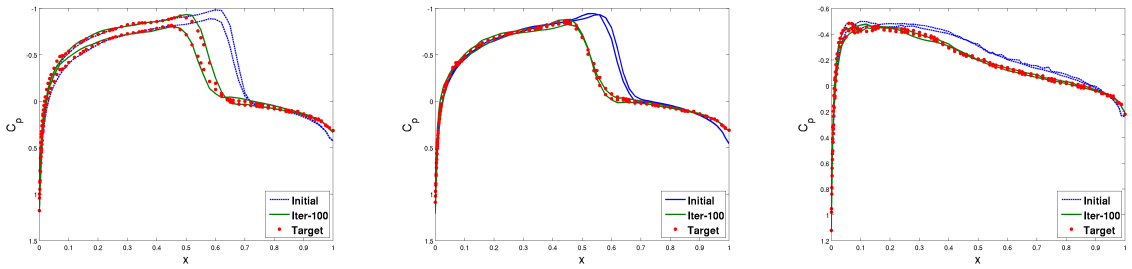

(a) Wing root (b) Wing station at 60% of the semi-span (c) Wing tip

Figure 18. Pressure distributions for rectangular wing test case at M = 0.85, wing with symmetric target wing profiles and twist angles varied linearly from 1° at the root to -1° at the tip, $\alpha = 0^\circ$

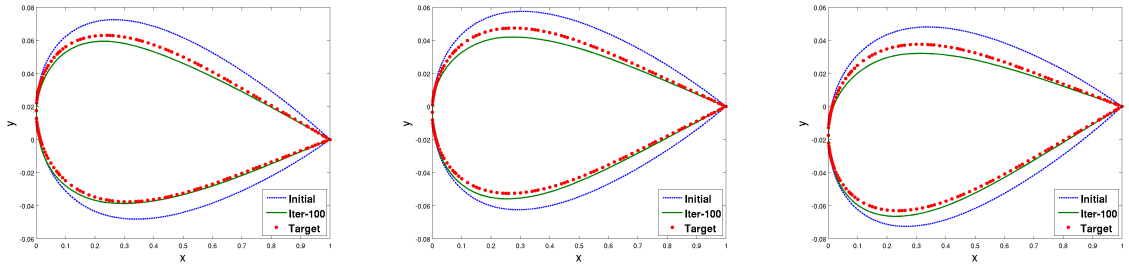

(a) Wing root (b) Wing station at 60% of the semi-span (c) Wing tip

Figure 19. Airfoil coordinates for rectangular wing test case at M = 0.85, wing with symmetric target wing profiles and twist angles varied linearly from 1° at the root to -1° at the tip, $\alpha = 0^\circ$

V. Optimization *D*iscussion *G*roup Test Cases

A. Test case I: drag minimization of the NACA0012 in transonic inviscid flow

The Test Case I from Optimization DG is the application to airfoils. The problem is to minimize the wave drag at inviscid flow with Mach 0.85 at zero angle of attack. The shape is constrained: its thickness must not be less than that of the baseline NACA0012. A very rough target pressure is generated using Campbell's method[2] without smoothing it. The initial airfoil has around 46 drag counts. As the pressure distribution is proceeding to the target, the drag decreases. After 30 iterations the drag is reduced to 23 counts. Further reduction of the drag is possible with more detailed and well-designed target pressure distribution. Vassberg et al.[19] report good results on drag reduction. Comparing our target pressure distribution (Figure 20(a)) with Vassberg's optimal pressure distribution, we can see a peak (minimum C_p) around the leading edge. We believe that wave drag is sensitive to airfoil nose curvature and the shape differences there are responsible for the drag difference.

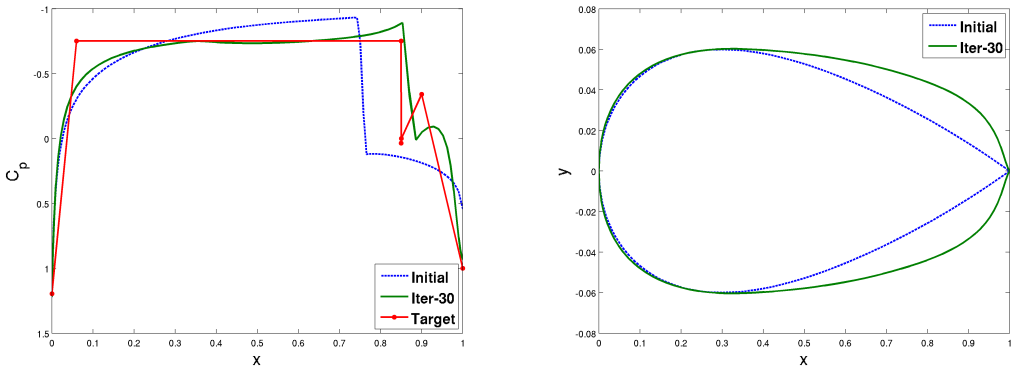

(a) Pressure distributions (b) Airfoil coordinates

Figure 20. Comparison of NACA0012 airfoil and its design *Iter-30* at transonic speed, M = 0.85, $\alpha = 0^\circ$

B. Test case II: wing twist optimization

For this test case a straight rectangular wing[15] with $AR = 6$ is studied. The optimization problem is

$$minimize: \ C_D(\gamma, u(\gamma)) \tag{14}$$

$$s.t.: \ C_L(\gamma, u(\gamma)) = 0.375, \frac{d\gamma}{dy}(y = 3c) \geq -10^\circ/c \tag{15}$$

where c is the chord length, the twist is denoted by γ, and the state variables by $u(\gamma)$. The flow condition is subsonic at Mach 0.5. The minimum mesh off-wall spacing is $0.004c$ with 3.7 M nodes. By specifying the local lift C_{LL} to be elliptic to minimize induced drag, the twisted wing is found by matching the C_{LL}[7,21] after four design cycles. The span efficiency factor $e = \frac{C_L^2}{\pi \lambda C_D}$ is already high for the initial untwisted wing, and twisting the wing sections can only improve it marginally. Four design cycles were made, it shows a good convergence towards the design target. Fig. 21 shows the results for optimizing the twist of a rectangular wing to minimize the induced drag, or, with target that produces an elliptical lift distribution. We can see that the span efficiency factor e converged to a higher value after four iterations (G04).

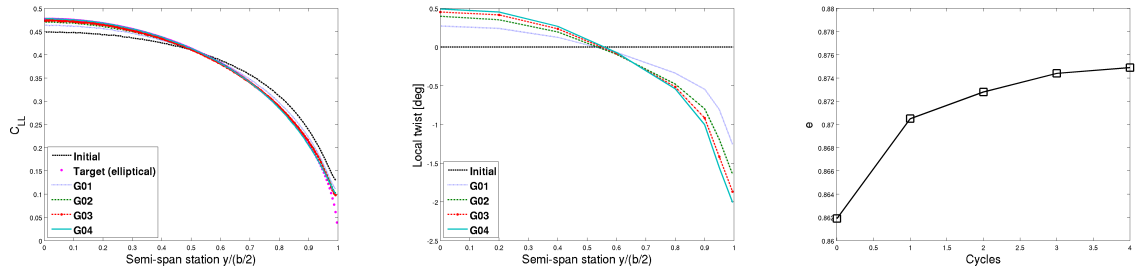

(a) Lift distributions

(b) Twist angle in degrees along the semi-span

(c) The convergent history of the span efficiency factor e

Figure 21. Results for optimizing the twist of a rectangular wing with NACA0012 profiles and $AR = 6$, M = 0.5, $C_L = 0.375$, angle of attack fixed at $\alpha = 4.26°$

Apparently by only twisting the wing it is difficult to significantly improve the wing's behavior. Letting engineer in loop becomes essential. Fig. 22 and 23 show the pressure distributions and their corresponding wing shapes obtained from classical wing inverse design method[21] by linear aerodynamic solver for the base configuration (left), optimized twisted wing (middle), and the twist-camber combined wing (right) when engineer is in the loop. The e factor at C_L ranges around 0.375 is further increased to a really high value $e \approx 0.97$ compared with the twist optimization configuration G04 where $e \approx 0.88$. We can see that for the twist-camber combined design, the leading edge spikes on the upper surface is much more flattened. Varying the twist alone may produce locally peaky C_p behavior along the span. The camber and twist should go together to get an optimized design from aerodynamic point of view. Peaky C_L designs even with good C_D may not be the best solution. Engineer needs to be involved into the design loop, other than only focuses on the numbers mathematically.

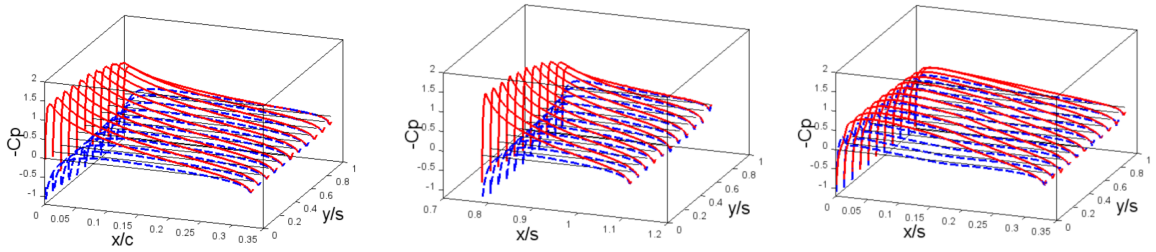

(a) Base configuration

(b) Twist optimization

(c) Engineer in loop, twist and camber variations

Figure 22. Pressure distributions from Nangia[21] inverse design method for designing a rectangular wing with $AR = 6$, M = 0.5, $C_L \approx 0.375$, engineer in loop

VI. Conclusions

Engineer in the loop to specify the C_p-distribution combined with an inverse design tool (SCID) is a promising approach. The SCID inverse design algorithm works for almost all the cases for airfoils, but needs further work on two issues, 1) cases with high lift and strong shocks; 2) the choice of user-defined

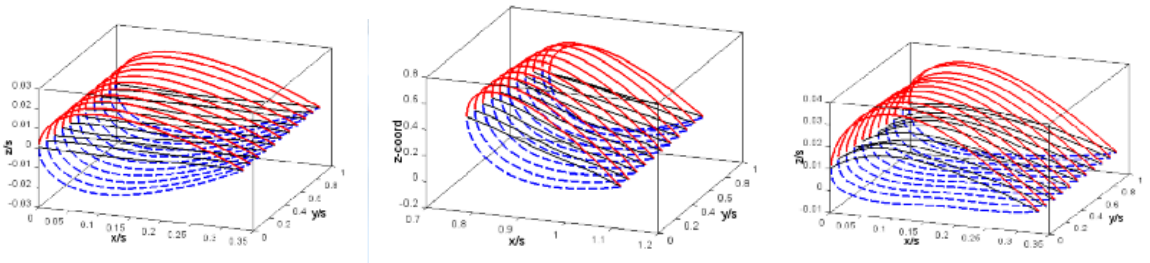

(a) Base configuration (b) Twist optimization (c) Engineer in loop, twist and camber variations

Figure 23. Wing section designs from Nangia[21] inverse design method for a rectangular wing with $AR = 6$, engineer in loop

coefficients. For wings there is limited success both for subsonic and transonic cases with predefined twists. Work is still on progress for the twist optimization. A more accurate relation between the shape and the pressure distributions C_p, such as can be furnished by solution of an adjoint equation, is being investigated.

VII. Future work

A more stable algorithm that works for wings with finite angle of attack at transonic is needed to investigate further. Also efforts must be made for defining a good target pressure distribution. One might follow Volpe's work[20] by combing with adjoint method to solve target pressure distributions. Speed acceleration can be made by adjoint with the mesh deformation for CFD calculation instead of re-meshing.

A. DG Test Case III: CRM model

The wing design involves three-dimensional design parameters in addition to the profile shape such as sweep, taper, dihedral and the local twists. The other is the Common Research Model (CRM) wing extracted from the given IGES file.[17] The mesh for solving the Euler equation has 0.24 M nodes. The design stations are at 0% (root), 30% (kink), and 99.5% (tip) of the semi-span. The far-field radius is more than 200 chord lengths.

The CRM model has not been investigated so much for the real twisted case. Figure 24 and 25 show the inverse design results using SCID with the target produced by the CRM planform without twist at Mach 0.85 with zero angles of attack. SCID works fine at transonic for untwisted wing even the wing is swept. It indicates that the SCID can deal with strong cross flow and we probably do not need the span-wise terms.

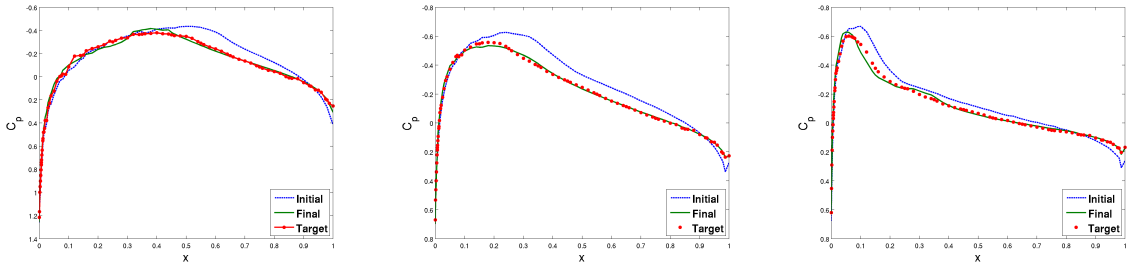

(a) Wing root (b) Wing station at the kink (30% of the semi-span) (c) Wing tip

Figure 24. Pressure distributions for CRM untwisted wing, at M = 0.85 with $\alpha = 0^\circ$

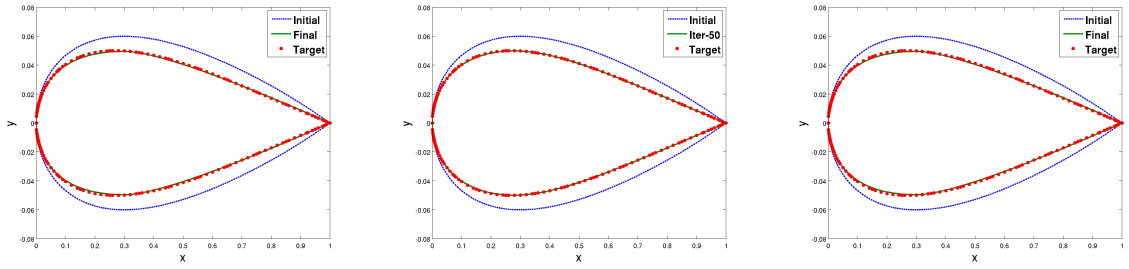

(a) Wing root (b) Wing station at the kink (30% of the semi-span) (c) Wing tip

Figure 25. Airfoil coordinates for CRM untwisted wing, at M = 0.85 with $\alpha = 0°$

B. Optimization on a real wing

We must do the optimization on a real wing, not the rectangular one for test. A real wing is, (most likely) swept, tapered and twisted. The section profiles may vary and is not necessarily to be symmetric. One good example is the CRM wing stated above. To accomplish the optimization, we need:

(a) make sure SCID works fine with all the cases for wings, or, try to finish case 6 in Table 2;

(b) introduce sweep and taper to the test wing;

(c) figure out the target C_p^* for the given wing planform.

For (a), one needs to think about how to allocate/distribute the local α and camber for a given C_p produced; for (b) is easier that we might apply the simply sweep theory and yaw the C_p;[16] for (c), one way to figure out the target C_p is to use adjoint for gradient calculation introduced by Volpe.[20]

References

[1]Campbell, R. L. and Smith, L.A., A hybrid algorithm for transonic airfoil and wing design, AIAA paper 87-2552, 1987.

[2]Campbell, R. L., An approach to constrained aerodynamic design with application to airfoils, NASA TP 3260, 1992.

[3]Takanashi, S., An iterative procedure for three-dimensional transonic wing design by the integral equation method, AIAA paper 84-2155.

[4]Drela,M., Newton solution of coupled viscous/inviscid multielement airfoil flows. AIAA Paper 90-1470.

[5]www.foi.se/en/Customer–Partners/.../Edge1/Edge/

[6]Barger, Raymond L. and Brooks, Cuyler W., Jr., A streamline curvature method for design of supercritical and subcritical airfoils, NASA TN D-7770, 1974.

[7]Lamar,J.E., A Vortex-Lattice Method for the Mean Camber Shapes of Trimmed Non-coplanar Planforms with minimum Vortex Drag, NASA TN D 8090, Washington, D.C., 1976

[8]Dulikravich, G. S. and Baker D. P., Aerodynamic shape inverse design using a Fourier series method, AIAA 99-0185, 1990.

[9]Dulikravich, G. S., Aerodynamic shape design and optimization, AIAA 91-0476, 29th Aerospace Sciences Meeting, January 7-10, 1991/Reno, Nevada.

[10]Bartelheimer, W. An improved integral equation method for the design of transonic airfoils and wings, AIAA-95-1688-CP.

[11]Nadarjah S. and Jameson A., Studies of the continuous and discrete adjoint approaches to viscous automatic aerodynamic shape optimization, AIAA paper A01-31133, 2001.

[12]Jamenson A., Aerodynamic design via control theory, Journal of scientific computing, vol. 3, 1988, pp.233-260

[13]Eller, D., sumo: Surface Modeler, http://www.larosterna.com/sumo.html, accessed December 2013

[14]Si, H., TetGen: A Quality Tetrahedral Mesh Generator and a 3D Delaunay Triangulator, http://tetgen.berlios.de/, accessed December 2013

[15]Hicken, J. E., Aerodynamic design optimization workshop: twist optimization case, Jan 2013.

[16]Streit, T., Wichmann, G., Von Knoblauch Zu Hatzbach, F., Campbell, R., Implications of conical flow for laminar wing design and analysis, 29th AIAA Applied Aerodynamics Conference 2011, AIAA 2011-3808.

[17]Osusky, L. M., Zingg, D. W., Lift-constrained drag minimization of a wing allowing section and twist variation with flow governed by the Reynolds-Averaged Navier-Stokes equations, July 10, 2013.

[18]Melin, T., Amadori, K., and Krus, P., Parametric wing profile description for conceptual design, CEAS paper 2011.

[19]Vassberg, J. C., Harrison, N., Roman, D., and Jameson, A., A systematic study on the impact of dimensionality for a two-dimensional aerodynamic optimization model problem. Number AIAA 2011-3176 in 29th AIAA Applied Aerodynamics Conference, Honolulu, Hawaii, June 2011, AIAA.

[20]Hayashi, M., Ceze,M., Volpe, E., Characteristics-based boundary conditions for the Euler adjoint problem, Int. J. Nuer. Meth. Fluids 2012; 00:1-30.

[21]Nangia, R. K., Palmer, M. E., and Doe, R. H.,"Aerodynamic Design Studies of Conventional & Unconventional Wings with Winglets", AIAA 2000-3400, 2000.

[22]Anderson, J. D., Modern Compressible Flow with Historical Perspective, Third Edition, International Edition 2004, ISBN 007-124136-1.